Shear transformation zone dynamics model for metallic glasses incorporating free volume as a state variable

Lin Li[1], Eric R Homer[2], Christopher A Schuh[1]

1. Department of Materials Science and Engineering, Massachusetts Institute of Technology, 77 Massachusetts Avenue, Cambridge, MA 02139, USA
2. Department of Mechanical Engineering, Brigham Young University, 435 CTB, Provo, UT 84602

Abstract

A meso-scale model, shear transformation zone dynamics (STZ dynamics), is employed to investigate the connections between structure and deformation of metallic glasses. The present STZ dynamics model is adapted to incorporate a structure-related state variable, and evolves via two competing processes: STZ activation that creates free volume vs. diffusive rearrangement that annihilates it. The dynamical competition between these two processes gives rise to an equilibrium excess free volume that can be connected to flow viscosity via the phenomenological Vogel-Fulcher-Tammann relation in relaxed structures near the glass transformation temperature. On the other hand, the excess free volume allows glasses to deform at low temperatures via shear localization into shear bands, even in presence of internal stress distributions that arise upon cooling after processing.

Keywords:

Metallic glasses; Shear transformation zone; Free volume; STZ-dynamics model; Shear bands

1. Introduction

Metallic glasses exhibit a great variety of deformation behaviors depending upon conditions [1]. At low temperature and high stress, the deformation is highly inhomogeneous and the plastic strain is localized into shear bands. On the other hand, at high temperature and low stress, deformation is homogenous, exhibiting Newtonian flow rheology that gives way to exponential rheology as the stress rises. Homogeneous flow is also associated with significant transients that follow any change in conditions (i.e., stress). The details of how all these diverse behaviors are connected in metallic glasses pertain to the underlying deformation mechanism of local shear shuffling in the amorphous structure. In particular, the shear transformation zone (STZ) originally proposed by Argon [2] and further observed and studied widely in computational simulations [3 - 7], has been accepted as a "unit process" that underlies the deformation of metallic (and other) glasses. STZs are essentially local clusters of a few atoms that can rearrange collectively in response to a shear stress. This local rearrangement not only involves the displacement of atoms, but also an anelastic reconfiguration of atomic neighbors and a redistribution of free volume within the atomic cluster. This free volume redistribution is not only a transient process, but is also believed to involve local, permanent changes to the *excess* free volume. The local accumulation of excess free volume is believed to facilitate shear localization through local softening in the vicinity of previously deformed regions [2].

The concept of free volume as an important internal state variable for glasses predates the STZ description of glass deformation, beginning with developments by Cohen and Turnbull [8, 9]. They laid the groundwork for scalar free volume evolution equations that have been widely and successfully applied by experimentalists to explain relaxation behavior during glass formation from the super-cooled liquid regime [10 - 12]. In addition, Spaepen [13] extended this approach to glass deformation on the basis of two competing processes mediated by free volume: free volume creation due to atomic motions driven by a shear stress vs. free volume annihilation via diffusive rearrangement. This extended phenomenological model is capable of capturing the homogenous and heterogeneous deformation modes in metallic glass, and is especially useful for describing deformation transients.

Both the STZ (as a fundamental unit process for glass deformation), and free volume (as an internal state variable that evolves with time, temperature, stress and position), are simplified pictures of what actually happens in a glass. There is a vast spectrum of STZs and STZ-like atomic rearrangements that occur in deforming glasses, and this spectrum is only poorly understood at present [14 - 16]. And "free volume" is often used as a catch-all internal variable that subsumes a far greater complexity of internal states, including chemical and topological short- and medium-range order, atomic stresses and strains, etc. [17 - 19]. Neither picture (STZs or internal state variable) is yet fully worked out, and it is for this reason that simulation work on metallic glasses is essential to progress on understanding glass deformation [20]. There is an inherent lack of direct experimental approaches to these events in atomic glasses, and as such atomistic simulations provide many details of plasticity in metallic glasses that would otherwise be unavailable [21]. Yet, even though these simulations provide significant detail, they suffer from a

limitation in both length and time scales (typically a few tens of nanometers during a few tens of nanoseconds). Atomistic methods are therefore less useful to investigate large-scale events that occur over a long time scale, *e.g.* glass formation by cooling from the melt at realistic rates.

In this context, meso-scale modeling methods are needed to bridge the gap between atomistic simulations and experiments by averaging out atomistic effects and accounting only for an ensemble of characteristic events. Such approaches, on one hand, enable simulations to access larger scales, and on the other hand retain a description of elementary deformation physics. For example, Vandembroucq [22] proposed a *depinning* model to investigate long-range spatial and temporal correlations in 'depinned' local shear transition events. The critical stresses that lead to depinning can involve a stochastic distribution in order to account for the structural disorder of metallic glass. By introducing an age parameter that can vary yield stress distribution, the authors were able to show an age-dependent shear banding behavior. A *fluidity* model developed by Picard [23, 24] associated the characteristic transition times with deformation and relaxation and produced complex spatio-temporal patterns of transformation events.

"STZ dynamics" is another mesoscale model proposed by Homer and Schuh [25 - 27]. In this model a simulated metallic glass is partitioned into an ensemble of potential STZs that are mapped onto a finite element mesh. The activation of individual STZs is selected via the Kinetic Monte Carlo (KMC) algorithm originally introduced by Bulatov and Argon [28 - 30], which uses an energy-based yield criterion according to a Boltzmann probability, with local biasing from the stress state. As a consequence, the model incorporates a time scale and at the same time thermal effects, which are missing from other mesoscale models. The activation of STZs leads to stress and strain redistribution, which is solved accurately via the Finite Element Method (FEM). The updated elastic field resulting from STZ activations in turn affects the rate of subsequent activation events and thus the dynamical evolution of the system. With this framework, the model is able to capture the basic behaviors of metallic glasses, including high-temperature homogeneous flow, and low-temperature strain localization into shear bands.

One limitation of STZ dynamics as it has been implemented to date, however, involves the use of a single, fixed energy barrier for STZ activation, which cannot capture the mechanical effects of structural evolution (e.g. local structural hardening or softening) as the system evolves. One consequence of this limitation is that autocatalytic accumulation of structural change (as in the dynamic softening that leads to shear localization) is difficult to trigger. In fact, when disorder pre-exists in the internal stress fields of the system (e.g., due to cooling from the liquid state), the dynamical correlations between STZ activations are not large enough to overcome the internal stress fields (structural disorder) to allow STZ activations to correlate and form shear bands [26, 31, 32]. In prior STZ dynamics simulations shear bands are only seen when the initial configuration is uniform and free of structural noise [26], which is neither realistic for a glassy material nor in line with the perception that local structural softening is responsible for shear banding in glasses in the first place.

3

In this paper, our purpose is to continue the development of the STZ dynamics modeling framework by incorporating a structural state variable into it. In line with the above discussion, we introduce *excess free volume* into the STZ dynamics model of Homer [26] as a simple internal parameter that can track local structural change and allow for dynamical softening and hardening. We allow system evolution via two competing processes: free volume creations via STZ activation vs. free volume annihilation via diffusive rearrangement; the treatment is in the spirit of the original works by Argon and Spaepen [2, 13]. In what follows, we first present our basic modeling framework followed by a two-dimensional FEM implementation. Then we explore the interplay between evolution of excess free volume and metallic glass deformation over a range of thermal and mechanical loads. In particular, we show that excess free volume-assisted shear banding occurs at low temperature even in the presence of structural disorder in 'processed' samples.

2. Modeling framework

Our STZ dynamics model is built upon that of Homer and Schuh [25 - 27], and uses the same general apparatus comprising a finite element mesh and a KMC algorithm. Following Homer's 2D implementation, we define STZs on a 2D irregular triangular mesh, with each element and its immediate surrounding neighbors representing a potential STZ, as illustrated by A and B in Fig.1. At any given time step, one STZ is selected according to the KMC algorithm to participate in an activation event based on its local conditions (e.g., stress and temperature). Our main adaptation of the Homer model is to add an internal state variable, excess free volume. It is represented as a normalized volume fraction, f_v, and can vary from 0 to 1, i.e. $f_v = 0$ corresponds to no excess free volume above the average polyhedral volume V^* in a dense random hard sphere glass, while $f_v = 1$ is an upper bound corresponding to a state where an STZ can be activated without accumulating extra free volume [2]. The upper bound free volume, $\zeta \Omega_o$, is only a fraction of V^*. The factor ζ can vary from 0.1 to 0.6 for liquid metals based on Cohen's calculation [8].

In our implementation free volume is a local parameter, and has a single value for each element in the FEM mesh. In the most general sense it should be regarded simply as an internal state variable that characterizes "damage" in the structure, or the structural distance from equilibrium; it need not be interpreted in a literal sense as a volume. In fact, unlike true free volume, our f_v does not flow through the system from one material point to another; it is locally created or annihilated at each point with no regard for volume balance. Consequently, one can envision more complex models or state variables, but the present choice is viewed as presenting a good compromise between simplicity and capturing essential physical features of glass structural evolution.

In the following subsections we explain our models for accumulation and loss of free volume, followed by how these are implemented in the KMC algorithm.

2.1 Free Volume and STZ Activation

Free volume and STZ activation are inherently linked in our proposed model, and in fact the link is bidirectional: STZ activation causes free volume accumulation, while free volume in turn affects the activation of STZs. We treat these two aspects of the relationship in turn.

Following the view of Spaepen [13], we envision that the dilatation required during STZ activation is not totally transient in that it need not be eliminated immediately after the transition; rather it remains in a post-activation state until it may be reduced by diffusive rearrangement. Consequently, each STZ activation results in excess free volume creation given as

$$\Delta f_v^+ = \varepsilon_v \left(1 - f_v\right)$$

(1)

This expression is derived from one of Argon [2], where ε_v is the local transformation dilatation, and $(1 - f_v)$ corresponds to a first order correction dictating that more dilated regions accumulate less free volume upon STZ activation; a very rarefied volume of material with $f_v = 1$ can shear without any additional volume dilatation. When an STZ is activated, the increase in free volume in each of its elements is calculated according to Eq. (1).

The process of STZ activation is also affected by the presence of free volume, although it otherwise follows the framework developed by Homer [26]. STZ activation is treated as an Eshelby inclusion problem [33]; that is, following activation, the STZ transformation strain is accommodated elastically by both the STZ and its surrounding matrix. The activation barrier for shearing an STZ is taken from the model proposed by Argon [2, 34]:

$$\Delta F_{STZ}\left(f_v\right) = \Delta F_{shear} + \Delta F_{v0} \cdot g_{stz}\left(f_v\right)$$
$$= \frac{7 - 5\upsilon}{30\left(1 - \upsilon\right)} \mu(T)\gamma_0^2 \Omega_0 + \left[\frac{2\left(1 + \upsilon\right)}{9\left(1 - \upsilon\right)} \mu(T)\varepsilon_v^2 \Omega_0 + \frac{1}{2\gamma_0}\frac{\hat{\tau}}{\mu(T)} \mu(T)\gamma_0^2 \Omega_0\right] \cdot g_{stz}\left(f_v\right)$$

(2)

where υ, $\mu(T)$, and Ω_0 represent Poisson's ratio, temperature-dependent shear modulus, and activation volume of STZ respectively. The activation energy ΔF_{STZ} in turn can be decomposed into two parts: a f_v independent part, ΔF_{shear}, which is the strain energy associated with an STZ shearing by the characteristic shear strain γ_0; and a f_v dependent part, $\Delta F_{v0}\ g_{STZ}(f_v)$, in which we factor out the excess free volume dependence into a function $g_{STZ}(f_v)$. ΔF_{v0} incorporates the contributions from two parts: (1) a strain energy for a temporary dilatation to allow the atoms to rearrange into the sheared position; and (2) an energy required to freely shear an STZ, where

$\hat{\tau}$ is the interatomic shear resistance. Both the dilatation energy and shear resistance can be reduced by f_v through $g_{STZ}(f_v)$ [2], defined as:

$$g_{STZ}(f_v) = \left\{1 + \alpha\left[\varepsilon_v\left(1 - f_v\right)\right]^2\right\} / \left(1 + \alpha\varepsilon_v^2\right)$$ (3)

where α is a proportionality factor (~ 0.8 [2]). The quadratic $(1 - f_v)^2$ dependence comes from the fact that the activation free enthalpy increment due to a net activation dilatation $\varepsilon_v(1 - f_v)$ is proportional to the square of this dilatational strain term. Therefore $g_{STZ}(f_v)$ varies between 1 and $1/(1 + \alpha\varepsilon_v^2)$ as f_v goes from 0 to 1. The activation barrier $\Delta F_{STZ} = \Delta F_{shear} + \Delta F_{v0}$ used in the previous implementation of the STZ Dynamics model by Homer et al. [25-27], is retrieved when $f_v = 0$.

With a free volume dependent activation energy $\Delta F_{STZ}(f_v)$, the activation rate of a single potential STZ is given as

$$\dot{s}_{STZ} = \nu_{STZ} \exp\left(-\frac{\Delta F_{STZ}(f_v) - \tau\gamma_0\Omega_0/2}{kT}\right)$$ (4)

where τ, T are the local shear stress and temperature respectively; ν_{STZ} represents the attempt frequency along the reaction pathway and is on the order of the Debye frequency; and k is Boltzmann's constant.

2.2 Free Volume Annihilation via Diffusive Rearrangement

Existing excess free volume can also be annihilated through diffusive rearrangement. For the purposes of our STZ dynamics model, a diffusive rearrangement is viewed as a local event that involves a *nnihilation of excess free volume* as

$$\Delta f_v^- = \varepsilon_v f_v$$ (5)

This form is also suggested by Argon [2], and again contains a correction that acknowledges the fact that free volume can only be annihilated in proportion to how much of it is present in the

first place; if $f_v = 0$ then no free volume reduction is possible. In our implementation, the local diffusional rearrangement associated with Eq. (5) occurs over small regions of exactly the same size and shape as potential STZs, and when such an event is triggered Eq. (5) is applied to every element in the selected zone (without applying any shape change).

The activation energy required to trigger a single event of excess free volume annihilation can be written as

$$\Delta G_D(f_v) = \Delta G_{v0} g_D(f_v) \tag{6}$$

where ΔG_{v0} is the activation free energy for a net diffusive rearrangement in a region with $f_v = 0$. $g_D(f_v)$ is a factor that lowers the energy barrier in a region containing excess free volume, which, again following Argon [2] is taken as $g_D(f_v) = (1 - f_v)$.

Therefore the activation rate of a single diffusive rearrangement event can be written as

$$\dot{s}_D = (1 - f_v) \nu_D \exp\left(-\frac{\Delta G_D(f_v)}{kT}\right) \tag{7}$$

Here the prefactor $(1 - f_v)$. represents another correction for reducing annihilation rate in proportion to the amount of free volume available to annihilate, while ν_D is the frequency factor for diffusive rearrangement.

2.3 Kinetic Monte Carlo

1. A KMC algorithm is employed to control the evolution of the system through a series of individual events selected according to their corresponding activation rates. The algorithm essentially follows the form originally proposed by Bulatov and Argon [28-30] and modified by Homer [26], but here we introduce two types of events (STZ activation vs. diffusive rearrangement) that are all enumerated and compete with each other through their activation rates. In each KMC step:

1. The activation rates for both processes, $\dot{s}_{STZ,i}$ and $\dot{s}_{D,i}$, at each potential site i are determined by Eq. (4) and Eq. (7) respectively.

2. These individual rates are then accumulated into a list and summed over the list such that the cumulative activation rate $\dot{s}_{tot}$, gives the rates for both processes over all i. For each site i, there are two normalized rates, which are given by

$$\eta_{STZ,i} = \dot{s}_{STZ,i} / \dot{s}_{tot}; \quad \eta_{D,i} = \dot{s}_{D,i} / \dot{s}_{tot} \tag{8}$$

such that

$$\sum_i \left(\eta_{STZ,i} + \eta_{D,i} \right) = 1 \tag{9}$$

3. Two random numbers ξ_1 and ξ_2 are generated within a uniform distribution on the interval (0, 1).
4. ξ_1 is employed to determine the elapsed time of the system by

$$\Delta t = -\ln \xi_1 / \dot{s}_{tot} \tag{10}$$

5. ξ_2 is to select the particular process and location for the next event. This is done by comparing the random number ξ_2 to the list of activation rates. If the random number falls in the range

$$\sum_{i=1}^{k-1} \left(\eta_{STZ,i} + \eta_{D,i} \right) < \xi_2 \leq \sum_{i=1}^{k-1} \left(\eta_{STZ,i} + \eta_{D,i} \right) + \eta_{STZ,k} \tag{11}$$

Then shear distortion γ_o is applied to the selected region i in a particular direction that is determined by the location of the random number ξ_2 on the subinterval associated with the stress state [26]. Additionally f_v increases in the region by an amount determined by Eq. (1). Otherwise, if the random number falls in the range

$$\sum_{i=1}^{k-1} \left(\eta_{STZ,i} + \eta_{D,i} \right) + \eta_{STZ,k} < \xi_2 \leq \sum_{i=1}^{k} \left(\eta_{STZ,i} + \eta_{D,i} \right) \tag{12}$$

then the diffusive rearrangement process for a particular activation region k is selected. In this case f_v decreases in the activation region k by the amount determined by Eq. (5).

6. After a transition occurs, either STZ activation or diffusive rearrangement, new stress and strain fields are solved by FEM.

These KMC steps can be repeated as many times as desired to simulate a given process, and the stochastic nature of the algorithm will produce a realistic outcome as long as the rates

governing the individual events are correct. The two possible events described in Step 5 are exclusive; in each KMC increment, only one of them will be selected.

2.4 2D FEM Implementation

We implement the STZ-dynamics model in the commercial finite element package ABAQUS via its user subroutines, and employ its FEM solver to determine the stress and strain fields as well as the evolution of the state variable (i.e. excess free volume) for each KMC increment.

Figure 1 shows the 2D FEM mesh used for the present simulations. Plane-strain quadratic triangular elements (CPE6MT) are employed, and the average potential STZ or diffusive rearrangement region contains 13-elements (refer to STZ A in Fig.1), with each potential STZ centered on an element and including all the neighbors that share its nodes. The number of potential STZs is thus equal to the number of elements, so there are total of 14846 potential STZs defined over 14846 elements in Fig. 1. The validation of this geometrical STZ mapping onto the FEM mesh is discussed by Homer [26], who showed that the 13-element STZ gives a reasonable compromise between solution accuracy (in terms of convergence) and computational speed. It is also worth noting that any element can participate in multiple STZs, which is physically reasonable since atoms may participate in multiple STZ events. Under this mapping rule, there are a few STZs that may contain more or less than 13 elements (ref. to STZ B in Fig. 1) depending on the local mesh.

For thermal excursions, the boundary conditions as shown in Fig. 1 are applied with no tractions on the sample surfaces. For mechanical loading, a case of pure shear is applied, and a corner node is fixed to remove the rigid body motion (refer to Fig.1). During the simulations, temperatures are kept uniform throughout the system.

2.5 Discussion of the modeling approach

At present, the newly introduced excess free volume represents a relatively simple way to incorporate a structural state variable into the STZ dynamics model. As will be shown in this work, this simple addition provides significant insight into the flow of excess free volume and its effects on glass deformation. However, the present implementation does have certain limitations that need to be addressed as knowledge of atomic scale deformation in glasses improves. For example, the present model creates and annihilates excess free volume locally; future work must focus on the diffusion of this free volume rather than the creation and annihilation thereof. Additionally, the excess free volume is a phenomenological variable like those used in most of the mesocale models [23, 31 – 32, 41]; one could develop similar approaches that connect to alternative state variables such as local elastic properties [42], local bonding such as icosahedral or non-icosahedral effects [14]; or dynamical state variables such as an effective disorder temperature [43 – 45]. Each of these state variables provide something unique to describe structural disorder of glasses, and the complex structural evolution in

metallic glasses provides freedom in the selection and description of variables to describe similar behaviors.

2.6 Simulation Parameters

Table 1 summarizes parameters used in the STZ dynamics simulations. For the sake of simplicity, we assume the STZ attempt frequency is equal to that for diffusive arrangement ($\upsilon_{STZ} = \upsilon_D$). The activation barrier for diffusive rearrangement is taken to be equal to the excess free volume-dependent part of STZ activation energy, i.e. $\Delta G_{v0} = \Delta F_{v0}$, considering that it is a volume related process. Additionally, the mechanical properties of Vitreloy 1 derived from experiments [35] are used.

3. Model output

We now exercise the model to briefly examine the role of excess free volume in metallic glass deformation, with the intent of evaluating its reasonableness. In this section, we first investigate the local evolution of excess free volume at the STZ level via the creation and annihilation processes. Samples are then processed via simulated heat treatment to obtain relaxed structures at various temperatures. Finally, samples with various internal structures are deformed through creep tests at high and low temperatures and the effect of excess free volume on the deformation processes is analyzed.

3.1 Local Free Volume Evolution

We start the simulations by tracking the performance of the two competing processes, i.e. free volume creation vs. annihilation. For a simple demonstration, a sample initially at a state of zero internal stress and zero excess free volume is loaded with a shear stress of 1 GPa at 300 K. Fig. 2a displays the resultant evolution of the macroscopic shear strain and the volume-average excess free volume, f_v: following a transient period, both shear strain and f_v rapidly increase as a consequence of strain localization into a shear band, which is illustrated in the insets (i.e., the spatial distribution of STZ strain and excess free volume at point A).

For further details, we zoom in and explore the local free volume evolution of a randomly selected element in the shear band (marked as a star in the insets of Fig. 2a), f_v^{ele}, the behavior of which is displayed in Fig. 2b. Over the course of the simulation, this particular element only occasionally participates in an STZ or diffusive event, so there are many fallow periods in which other activity is occurring. For example, this STZ is the third to be activated at the outset of the simulation, and at a time of about 40 Gs after loading f_v^{ele} dramatically increases from 0 to 0.5 upon this first activation. However, immediately after, f_v^{ele} drops by half to 0.25, and then after a short period drops by half again to 0.125 as a result of annihilation processes. This is a pattern that is common in the present model, where a single deformation event causes large rises in excess free volume, in turn leading to a significantly reduced activation barrier for relaxation

some short time later. The history of local free volumes is replete with such peak-and-decay patterns.

Even once deformation accelerates during a localization event, the same local pattern is revealed; near the time marked by A, the evolution of the excess free volume accelerates and numerous creation and annihilation events are selected within very short time intervals; the inset to Fig. 2b shows that this selected STZ is activated four times with numerous relaxations in between over the course of this acceleration period. This acceleration in local evolution of f_v^{ele} is directly associated with the macroscopic strain evolution as shown in Fig. 2a, where we observe that this is the time where strain begins to rapidly localize into a shear band.

This exercise illustrates that f_v^{ele} is determined by dynamic balancing between creation and annihilation. Annihilation occurs more frequently because its activation energy barrier is lower and is more significantly reduced by the existing f_v^{ele} (ref. to Eq.(6)). Usually one creation event is followed by 2 ~ 4 annihilation events, which is consistent with Spaepen's assessment that the number of diffusive jumps necessary to annihilate excess free volume is between 1 and 10 [13].

3.2 Thermal Treatment (Structural Relaxation)

Due to their disordered structure, metallic glasses contain a distribution of internal stresses [14], and in STZ dynamics such distributions arise entropically upon thermal processing. The development of such a distribution from an initially stress-free state is illustrated in Fig. 3a where the instantaneous elastic strain energy density in the system is plotted as a function of time for various annealing temperatures, under zero applied stress. Fig. 3a provides a comparison of the timescales required to anneal at different temperatures as well as the equilibrium strain energy density that is achieved at each temperature. Note that the logarithmic scale on the time axis obscures the achievement of a steady state for each annealing temperature, which can be better illustrated by plotting the strain energy density as a function of the KMC steps, as illustrated by the inset for the 650 K simulation. A plot of the equilibrium elastic strain energy density values for each of the simulations shows a linear relationship with the temperature as displayed in Fig. 3b. This linear trend is well established from 500 to 1000 K and has an extrapolated intercept of 0 ± 200 kJ·m^{-3} at 0 K.

During annealing the excess free volume evolves as well, as shown for various annealing temperatures in Fig. 4a. Upon annealing, f_v increases dramatically, and saturates earlier than the corresponding elastic strain energy density. Thereafter f_v oscillates around an equilibrium value $f_{v,eq}$, and the amplitude of oscillation increases with annealing temperature as a consequence of thermal fluctuations. An example of f_v vs. KMC steps at 650 K is displayed as an inset to better illustrate the achievement of a steady state.

11

The annealing process produces an asymmetric distribution of f_v^{STZ} at steady state, as shown more explicitly in Fig. 4b. This asymmetric distribution is somewhat like the exponential distribution proposed in the free volume theory [8] with a large fraction of small f_v^{STZ} balanced by a small fraction of large f_v^{STZ}. Furthermore, the f_v^{STZ} distribution in turn leads to a distribution of activation energy barriers for the two competing processes, as shown in Fig. 4c. Both activation energy barrier distributions take on a similar shape, yet the diffusive process ΔG_D is situated at smaller energy values and has a broader distribution in comparison to the STZ activation barrier ΔF_{STZ}.

The distributions in Fig. 4c reflect the disordered nature of glass structure in our model. They are not explicitly input to the model, but are emergent distributions that can evolve with deformation and processing. While this is an interesting contrast to other mesoscale models [32] that include a distribution of events a priori, it also reveals a significant point of departure between the present simple model and the true internal structure of a metallic glass. In comparison to the STZ activation energy distributions measured by Argon via mechanical spectroscopy [36], our ΔF_{STZ} distributions have a similar shape, but they are very much narrower (~ 0.1 eV) than the experiments (~ 1 eV). Similarly, the activation energy distribution calculated by the atomistic simulations [16] again exhibits an energy spectrum that is much broader (~ 1 eV). This result points to a greater need for an improved state description, which may ultimately be provided by multiscale modeling.

The equilibrium volume-average excess free volume $f_{v,eq}$ at various annealing temperatures is plotted in Fig. 5. The simulated $f_{v,eq}$ vs. temperature is strikingly linear, and can be well described by a fitted relationship:

$$f_{v,eq} = \alpha_{fv}(T - T_0).$$
(13)

This form is the one familiar from free volume theory [37, 38], although it is important to note that no input to the present model specifically built in the linear form of Eq. (13). The slope α_{fv} = 7.4 x 10^{-5} K^{-1} is a measurement of increase in $f_{v,eq}$ with respect to temperature, and T_0 = 280 K is the temperature at which $f_{v,eq}$ reaches 0. These values can be compared to those experimentally reported for Vitreloy 1 [11]. T_0 = 426.3 K is the Vogel-Fulcher-Tammann (VFT) reference temperature of Vitreloy 1, which is somewhat higher with the present simulated value of 280 K. To make a comparison with regard to α_{fv}, we recall that the experimentally measurable quantity is $\alpha_v = \zeta \alpha_{fv}$, with ζ in the range 0.1 ~ 0.6. Correspondingly, the range for α_v from our simulations is 7.4 x 10^{-6} to 4.5 x 10^{-5} K^{-1}. For Vitreloy 1, $\alpha_v = \alpha_{liq} - \alpha_{glass}$ = 1.93 x 10^{-5} K^{-1}, (i.e., the difference in thermal expansion coefficients between the liquid and the glass [37]), which falls in the middle of the simulation range.

12

Considering that no assumption is made on the temperature dependence of $f_{v,eq}$ in the simulations or their inputs, the value of α_{fv} is an emergent property of the model with important implications for glass structure and deformation. It is encouraging that the model can reproduce the form of Eq. (13) with a reasonable match to experimental data, especially since the temperature dependencies that went into the model as input are not linear, but exponential. To appreciate how a linear form can emerge, it is instructive to examine the equilibrium condition of the present model, by setting equal the rates of free volume increase and decrease:

$$\varepsilon_v\left(1 - f_v\right)\nu_{STZ}\,\exp\!\left(-\frac{\Delta F_{STZ} - \tau\gamma_0\Omega_0}{kT}\right) = \varepsilon_v f_v\left(1 - f_v\right)\nu_D\,\exp\!\left(-\frac{\Delta G_D}{kT}\right) \tag{14}$$

In the true equilibrated glass, there is a wide distribution of local stress states and free volumes, but as the simplest approximation we may replace the local state variables with global average values ($\tau = 0$ during annealing). Given our prior assumption that $\nu_{STZ} = \nu_D$, we then have

$$f_v = \exp\!\left(-\frac{\Delta F_{STZ}(f_v) - \Delta G_D(f_v)}{kT}\right) \tag{15}$$

where both ΔF_{STZ} and ΔG_D depend on f_v. Eq. (15) provides an implicit relationship between $f_{v,eq}$ and temperature, is plotted in Fig. 5 using the simulation input parameters as a red solid line. This simple equilibrium model agrees reasonably with the full simulation output, and most importantly, exhibits a broad apparently linear regime at higher temperatures, much as the simulation results do. While this expression is not linear, it is instructive to see that on the relevant scales of the present problem, it can appear so; this provides some support for the use of Eq. (13) in describing the free volume state of an equilibrated glass.

We may linearize Eq. (15) by assuming (as we have done in the simulations) that $\Delta F_{v0} = \Delta G_{v0}$, and performing a Taylor expansion about a characteristic temperature (T_0) and free volume (f_{v0}). This leads directly to Eq. (13) with the following values of the parameters:

$$\alpha_{fv} = \frac{k\ln^2(f_{v0})}{\Delta F_{shear}/f_{v0} + \Delta F_{v0}\left(\dfrac{1 - \alpha\varepsilon_v^{\,2}}{1 + \alpha\varepsilon_v^{\,2}}\left(1 - \ln(f_{v0})\right) + f_{v0}\,\dfrac{\alpha\varepsilon_v^{\,2}}{1 + \alpha\varepsilon_v^{\,2}}\left(1 - 2\ln(f_{v0})\right)\right)} \tag{16a}$$

13

$$T_0 = \frac{-\Delta F_{shear}(1+\ln(f_{v0})) - \Delta F_{v0}\left(\dfrac{1-\alpha\varepsilon_v^{\,2}}{1+\alpha\varepsilon_v^{\,2}}f_{v0} + \dfrac{\alpha\varepsilon_v^{\,2}}{1+\alpha\varepsilon_v^{\,2}}(1-\ln(f_{v0}))f_{v0}^{\,2}\right)}{k\ln^2(f_{v0})} \qquad (16b)$$

By choosing a reference free-volume content f_{v0} =5% that would be generally characteristic of the super-cooled liquid region, Eq.(16) gives α_{fv} = 9.3 x 10^{-5} K^{-1} and T_0 = 405 K. This linearization is the one shown in the broken black line in Fig. 5; the slope matches reasonably with the simulations, while the characteristic temperature is somewhat higher than that given by extrapolation of the simulation data (T_0 = 280 K) but in better agreement with the experimental value (T_0 = 426.3 K). The fact that our equilibrium free volume follows the expected empirical linear relationship with respect to temperature, to some extent, validates our dynamical rules for the free volume evolution. It also provides some insight into the possible origins of these empirical relationships, which in turn provides some support for many continuum models that assume their validity a priori.

3.3 High-Temperature Rheology

The high-temperature deformation behavior of the relaxed structures is studied over a range of stresses at different constant temperatures near and above T_g = 623 K (the glass transition temperature of Vitreloy 1 [35]). In all the simulations, pure shear traction is applied and held at a constant value. Fig. 6a-c show the shear strain vs. time data over a range of stresses at 650 K, and the corresponding evolutions of f_v are displayed Fig. 6e-g. At lower stresses (Fig.6a & 6e) a steady state flow is established almost instantaneously with a constant strain rate and minor change in f_v of the same scale as its thermal fluctuation range. As stress increases to 500 MPa (Fig. 6b & 6f), the transients become more significant, especially in f_v, which shows a dramatic increase followed by a relatively quick saturation at a steady-state value. Since f_v saturates so quickly, the transient in structural adjustment does not give rise to a noticeable transient in the strain response. As the applied stress continues to increase to 1 GPa (Fig. 6c & 6g), a longer-lived transient in both variables is observed. The spatial distributions of STZ strain as well as f_v at the time marked t_1 (in the transient) and t_2 (nearing the steady-state) are provided in Fig. 6d & Fig. 6h respectively. At t_1 in Fig. 6h, f_v is distributed heterogeneously, with only fraction of the sample having increased values. On the other hand, at t_2 the higher level of accumulated free volume f_v is distributed homogenously throughout the sample, as is the strain (ref. to Fig. 6d)

For each of the different simulations in Fig 6 and many others like them, the steady-state strain rate is assessed and compiled in Fig. 7a as a function of the applied stress. The datasets show typical homogeneous glass flow for metallic glasses at high temperatures, that is, weakly rate-dependent Newtonian behavior at low stresses vs. non-Newtonian flow with gradually

enhanced rate sensitivity at high stresses. This high-temperature flow generally conforms to the classical one-dimensional model of independent forward-and-backward STZ activation [13]. A simple combination of the forward and backward rates of Eq. (4) results in a hyperbolic-sine stress-dependence to the steady state strain rate

$$\dot{\gamma} = 2 \cdot \gamma_0 \cdot \nu_{STZ} \exp\left(-\frac{\Delta F_{STZ}(f_v)}{kT}\right) \sinh\left(\frac{\tau\gamma_0\Omega_0}{2kT}\right) \tag{17}$$

In principle, this one-dimensional model contains the same inputs that our 2D simulations do, so it can be compared to the simulation output without the use of any adjustable parameters. This is presented in Fig. 7a, where the agreement between the data and Eq. (17) is good, especially as regards the general locations of the Newtonian regime at low stresses and its divergence into exponential flow at higher stresses.

Figure 7b shows a plot of the equilibrium value of the volume average excess free volume $f_{v,eq}$ as a function of applied stress at various temperatures. In the Newtonian flow region, $f_{v,eq}$ barely changes with applied stress, but there is a dramatic increase with applied stresses after entering the non-Newtonian flow region. The temperature effect on $f_{v,eq}$ is not at all significant on the scale here, and the small difference that does exist diminishes with increasing stress. Examination of the creation and annihilation processes of excess free volume f_v, one can write the time rate of change

$$\frac{df_v}{dt} = 2\varepsilon_v\left(1-f_v\right)\nu_{STZ} \exp\left(-\frac{\Delta F_{STZ}(f_v)}{kT}\right)\cosh\left(\frac{\tau\gamma_0\Omega_0}{2kT}\right) - 2\varepsilon_v f_v\left(1-f_v\right)\nu_D \exp\left(-\frac{\Delta G_D(f_v)}{kT}\right) \tag{18}$$

Note that the stress dependence of df_v/dt is hyperbolic-cosine rather than sine in Eq. (17). This is due to the fact that both forward and backward STZ operations can create excess free volume. Steady state is achieved when $df_v/dt = 0$.

The equilibrium $f_{v,eq}$ can be numerically solved from Eq (18), and is plotted in Fig.7d as solid lines. The match to the simulation data is good, although the predicted values are consistently higher, and this is accentuated at high stress. These discrepancies are most likely related to the free volume distribution in the simulations; when there is a distribution of options, STZs prefer operating more frequently at the locations with large f_v. These preferred operations, on one hand, will give rise to a fast flow rate; and, on the other hand, result in a small amount of f_v

increment (ref. to Eq. (4)), and thus relatively small f_v. The one-dimensional equilibrium model of Eq. (18) replaces the distribution with an average free volume and thus misses this detail.

We may further appreciate the structure-property connection of a deforming glass by considering the viscosity of glass flow in the super-cooled liquid region. Fig. 8 shows the viscosity in the Newtonian flow region at various temperatures vs. the corresponding steady-state excess free volume f_v. The viscosity is calculated as $\eta = \tau / \dot{\gamma}$ from the simulation data at 50 MPa in Fig. 7a. The apparently exponential form of the data in Fig. 8 is reminiscent of the classical Doolittle equation [38]:

$$\eta = \eta_0 \exp(\frac{b}{f_v}) \tag{19}$$

which is proposed to describe the flow of a glass in the homogeneous regime. Fitting our data into the form of Eq. (19) gives η_o = 1.58 and b = 0.64. Further, by taking into account the linear relationship between f_v and temperature that emerged earlier in our analysis in the form of Eq.(13), we obtain the Vogel-Fulcher-Tamman (VFT) equation:

$$\eta = \eta_0 \exp(\frac{b}{\alpha_{fv}(T - T_0)}) \tag{20}$$

As was noted earlier with reference to Eq (13), it is a nontrivial result that our simulations should conform to VFT kinetics, as the inputs to the model do not explicitly contain the VFT parameters α_{fv} and T_0 or the linear form of Eq (13). The VFT scaling is only apparently obeyed in our simulations as the consequence of two competing processes; this behavior is emergent.

3.4 Low-Temperature Deformation

Low-temperature deformation is examined in a structure that has been cooled at experimental rates to quench in a certain degree of disorder. This structure is achieved by starting with one equilibrated at 650 K (above T_g = 623 K of Vitreloy 1) and allowing the sample to evolve while it is cooled in the absence of external stress to 300 K at a rate of 10 K/s. The cooled structure is out of equilibrium because of the finite cooling rate, with an average excess free volume f_v = 0.026 that is significantly above that expected in equilibrium ($f_v \sim 0$, cf. Fig.5). The specimen is then tested in pure shear at 2 GPa at 300 K.

The resultant shear strain and volume average excess free volume f_v are plotted as a function of time in Fig. 9a. A significant transient period is clearly observed in both the shear strain and f_v responses. Early in this period (Fig. 9b), the internal stress distribution resulting from the thermal treatments inhibits STZs from activating in a correlated fashion, which is reflected in the randomly distributed spots with large f_v. These uncorrelated STZ activations are not associated with the development of significant plastic shear strain along the loading direction. Shortly thereafter, though, f_v responds and develops into a localized band of accumulation (Fig. 9c), well before strain begins to accumulate in a significant sense. This localized f_v band facilitates shear localization, and ultimately leads to a nascent shear band at the same location (Fig. 9d). Once the shear band forms, the localized shearing promotes rapid accumulation of plastic deformation (from Fig. 9d to Fig. 9e); meanwhile f_v increases at a roughly constant rate as the shear band widens. Over the entire process, the f_v band propagates ahead of the shear band, which is further illustrated by the 1D STZ and f_v distribution plots in Fig. 9b - e. We conclude that excess free volume catalyzes shear localization. The softening that often precedes localization into a shear band has been observed previously when structural relaxation and local softening are accounted for [32, 39-40].

The ability to observe shear localization in samples with pre-existing structure is an important improvement to the STZ dynamics model [26]. Fig. 10 shows the shear strain evolution of the same cooled structure under the same loading conditions (i.e., at 300 K and 2 GPa) as Fig. 9, but now after having turned off the free volume evolution. As reported by Homer et al. [26], rather than forming shear band, the sample undergoes homogenous deformation without the assistance of free volume. The addition of the structural state variable allows the system to localize due to structural memory that is retained even after the redistribution of stress, and allows the system to facilitate correlated events to overcome the noise induced by the internal stresses and dictate individual STZ operation into shear band. In future work we hope the model can be exploited to study shear band formation and propagation kinetics.

4. Conclusions

We further developed the STZ dynamics simulation method for glasses [25-27] by incorporating a structural state variable that can allow for dynamical hardening and softening of a disordered solid upon heating or deformation. We specifically develop a model on the basis of *excess free volume* as the internal variable, and new features added to the framework include:

- Excess free volume evolves via two competing processes: the STZ activation that creates free volume vs. the diffusive rearrangement that annihilates it. The activation unit of the two processes is taken to be a coarse-grained collection of atoms.
- At the same time, the excess free volume can in turn affect the two competing processes by modifying their activation energy barriers.

We implement the model in two dimensions, and perform a series of thermal and mechanical simulations that illustrate the interplay between the excess free volume evolution and the metallic glass deformation. The key results include:

- Over the course of structural relaxation at high temperatures, the excess free volume saturates faster than the corresponding elastic strain energy density. After reaching equilibrium, the excess free volume fluctuates around an equilibrium value with a magnitude that increases with annealing temperature.

- In equilibrium, the excess free volume takes an asymmetric distribution, in which a large fraction of small values is balanced by a small fraction of large values. In addition, a linear relationship can be established between the volume-average excess free volumes and the annealing temperatures, which is in line with classical free volume theory. The distribution of the excess free volume results in the distributions of the activation energy barriers of both STZ transformation and diffusive arrangement. The activation energy distributions take on a similar shape as experimentally measured ones [36], but are much narrower (~0.1 eV) than the measured ones (~ 1 eV).

- In shear loading at high temperature, the excess free volume first increases and then reaches a shear-enhanced equilibrium value in steady-state homogenous flow. At high stresses the excess free volume gradually increases to a steady state value an order of magnitude larger than the starting one. Both the shear rate and excess free volume in the steady-state follow expectations based on simple one-dimensional analytical models used widely to analyze glass rheology.

- Free volume catalyzes shear localization. For a quenched glass structure deformed at low temperature, strain localization into a shear band directly follows excess free volume accumulation in that band. This highlights a key improvement over previous STZ dynamics models, where localization could be suppressed by internal stress distributions.

References

[1]   Schuh C, Hufnagel T, Ramamurty U. Acta Mater, 2007; 55: 4067

[2]   Argon A S. Acta Metall Mater, 1979; 27: 47

[3]   Srolovitz D, Vitek V, Egami T. Acta Metall Mater, 1983; 31: 335

[4]   Deng D, Argon A S, Yip S. Philos T Roy Soc A, 1989; 329: 549

[5]   Falk M L, Langer J S. Phys Rev E, 1998; 57: 7192

[6]   Lemaître A. Phys Rev Lett, 2002; 89: 195503

[7]   Lund A C, Schuh C A. Acta Mater, 2003; 51: 5399

[8]   Cohen M H, Turnbull D. J Chem Phys, 1959; 31: 1164

[9]   Turnbull D. J Chem Phys, 1970; 52: 3038

[10]   Busch R, Bakke E, Johnson W L. Acta Mater, 1998; 46: 4725

[11]   Masuhr A, Busch R, Johnson W L. J. Non-Cryst. Solids, 1999; 250–252, Part 2: 566

[12]   Masuhr A, Waniuk T A, Busch R, Johnson W L. Phys Rev Lett, 1999; 82: 2290

[13]   Spaepen F. Acta Metall Mater, 1977; 25: 407

[14]   Egami T. Prog Mater Sci, 2011; 56: 637

[15]   Rodney D, Schuh C. Phys Rev B, 2009; 80: 184203

[16]   Rodney D, Schuh C. Phys Rev Lett, 2009; 102: 235503

[17]   Spaepen F. Scripta Mater, 2006; 54: 363

[18]   Falk M L. Phys Rev B, 1999; 60: 7062

[19]   Egami T. Intermetallics, 2006; 14: 882

[20]   Rodney D, Tanguy A, Vandembroucq D. Model Simul Mater SC, 2011; 19: 083001

[21]   Falk M L, Maloney C E. Eur Phys J B, 2010; 75: 405

[22]   Baret J-C, Vandembroucq D, Roux S. Phys Rev Lett, 2002; 89: 195506

[23]   Picard G, Ajdari A, Lequeux F, Bocquet L. Phys Rev E, 2005; 71: 010501

[24]   Martens K, Bocquet L, Barrat J-L. Phys Rev Lett, 2011; 106: 156001

[25]   Homer E R, Rodney D, Schuh C A. Phys Rev B, 2010; 81: 064204

[26]   Homer E R, Schuh C A. Acta Mater, 2009; 57: 2823

[27]   Homer R E, Christopher A S. Model Simul Mater SC, 2010; 18: 065009

[28]   Bulatov V V, Argon A S. Model Simul Mater SC, 1994; 2: 167

[29]   Bulatov V V, Argon A S. Model Simul Mater SC, 1994; 2: 185

[30]   Bulatov V V, Argon A S. Model Simul Mater SC, 1994; 2: 203

[31]   Jagla E. Phys Rev E, 2007; 76: 046119

[32]   Vandembroucq D, Roux S. Phys Rev B, 2011; 84: 134210

[33]   Eshelby J D. P Roy Irish Acad A, 1957; 241: 376

[34]   Argon A S, Shi L T. Acta Metall Mater, 1983; 31: 499

[35]   Johnson W, Samwer K. Phys Rev Lett, 2005; 95: 195501

[36]   Argon A S, Kuo H Y. J. Non-Cryst. Solids, 1980; 37: 241

[37]   Williams M L, Landel R F, Ferry J D. J Chem Phys, 1955; 77: 3701

[38]   Doolittle A K. J App Phys, 1951; 22: 1471

[39]   Manning M L, Langer J S, Carlson J M. Phys Rev. E. 2007; 76: 056106

[40]   Moorcroft R L, Cates M E, Fielding S M. Phys Rev Lett, 2011; 106: 055502

[41]   Zhao P, Li J, Wang Y, Int. J. Plast., 2013; 40: 11

[42]   Tsamados M, Tanguy A, Goldenberg C, Barrat J-L. Phys Rev E, 2009; 80: 026112

[43]   Langer J S., Scripta Mater, 2006; 54: 375

[44]   Bouchbinder E., Langer JS., Phys Rev Lett, 2011; 106: 148301

[45]   Bouchbinder E., Langer JS., Phys Rev E, 2011; 83: 061503

Table 1: List of simulation parameters used in free volume-assisted STZ dynamics simulations

| Simulation Parameters	Value
STZ attempt frequency	υ_{STZ} = 1.0193x10^{12} s^{-1} (ref. to Eq. 4)
Diffusive arrangement frequency	υ_D = 1.0193x10^{12} s^{-1} (ref. to Eq. 7)
Free volume-independent STZ activation energy	ΔF_{shear} = 0.9x10^{-30}J/Pa∗μ(T) (ref. to Eq. 2)
Free volume-dependent STZ activation energy	ΔF_{v0} = 8.1x10^{-30} J/Pa∗μ(T) (ref. to Eq. 2)
STZ shear strain	γ_o = 0.1 (ref. to Eq. 2 & 4)
STZ dilatational strain	ε_v = 0.5 (ref. to Eqs. 1,3 & 5)
STZ activation volume	Ω_o = 1.6 nm^3 (ref. to Eq. 2 & 4)
Temperature-dependent shear modulus	$\mu(T)$ = 37 GPa -0.004 GPa/K∗T (ref. to Eq. 2)
Poisson's ratio	ν = 0.352 (ref. to Eq. 2)

Figure Captions

Fig. 1: 2D FEM representation of a simulated sample. Region A is an example of a 13-element STZ that is prevalent in this 2D meshing. Region B is an exception that has 14 elements. Pure shear is applied when the sample is under mechanical loading. This image also shows the redistribution of von Mises equivalent stresses (shaded) when STZs A and B are activated.

Fig. 2: (a) The macroscopic shear strain and volume-average f_v evolution with respect to time. The insets show the contour plot of the spatial distribution of plastic STZ strain and f_v at the time marked A. The position of the selected element is marked as a star in the contour plots. (b) The local f_v evolution of the selected element over a series of activation events (marked by the points). The inset is a magnified view at marker A. This test is conducted at constant shear = 1 GPa and 300 K upon a stress-free sample with zero initial excess free volume.

Fig. 3: (a) The elastic strain energy vs. time for annealing at various temperatures. The inset shows an example at 650 K to confirm the convergence of this process to a steady state. (b) The elastic energy density in the equilibrated state vs. temperature.

Fig. 4: (a) The evolution of volume-average excess free volume f_v vs. time during annealing at various temperatures. The inset shows an example at 650 K plotting against KMC steps. (b) The distribution of f_v of each STZ when reaching steady state at various temperatures. The inset shows an example of the spatial distribution of f_v at 650 K. (c) The activation energy distribution in steady state for STZ activation, ΔF_{STZ}, and diffusive arrangement, ΔG_D.

Fig. 5: The equilibrium free volume at various temperatures from annealing simulations, plotted along with a linear relationship (ref. to blue dashed line) $f_{v,eq} = \alpha_{fv}(T - T_0)$, where α_{fv} = 7.44 x 10^{-5} K^{-1} and T_0 = 280 K. The numerical solution of Eq. (15) is shown in red; and its linearization is in black with α_{fv} = 9.43 x 10^{-5} K^{-1} and T_0 = 405 K obtained from Eq. 16 with a reference f_{v0} = 5%

Fig. 6: (a) - (c) The strain vs. time data for the creep response of a relaxed structure at various shear stresses at constant temperature 650 K. (e) - (g) The corresponding f_v evolution over the course of the creep tests. (d) The snapshots of STZ strains at marked time t_1 and t_2 in (c) for the case of shear stress = 1 GPa. (h) Two snapshots at the same time as (d) of the spatial distributions of f_v.

Fig. 7: (a) Steady-state homogenous flow data for several high temperature simulations, plotted along with the predicted strain rates from Eq.(17). **(b)** The equilibrium f_v at steady-state as a function of applied load for several high temperature simulations, plotted along with the predicted values from Eq.(18).

Fig. 8: The simulated viscosity in the Newtonian flow region at various temperatures vs. the corresponding excess equilibrium free volume f_v, plotted along with the fitted Doolittle equation, $\eta = \eta_0 \exp(\dfrac{b}{f_v})$, where $\eta_\circ$ = 1.58 and b = 0.64.

Fig. 9: (a) The shear strain and excess free volume f_v vs. time data of a cooled structure deformed at 300 K and 2 GPa shear load. **(b) - (e)** correspond to the snapshots at different times during the creep test. For each time, the physical deformation along with the magnitude of STZ strain and f_v are displayed; additionally a plot with 1D profile of STZ strain and f_v distributions along the vertical direction of the deformed sample is provided.

Fig. 10: The shear strain vs. time data of the same cooled structure under the same deformation conditions as in Fig. 9 (i.e., at 300 K and 2 GPa shear load) but after turning off the free volume evolution. The insets show the spatial distribution of STZ strain and the corresponding 1D profile of STZ strain along the sample vertical direction at the marked time, both of which illustrate the homogenous nature of deformation.
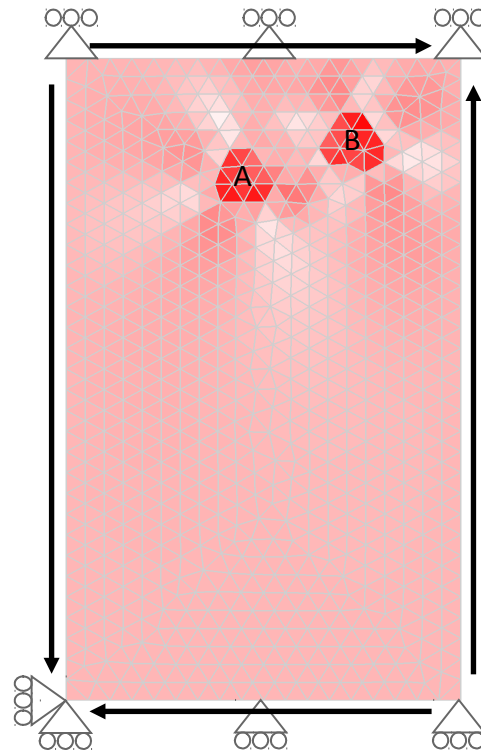
Fig.1: 2D FEM representation of simulation sample. Region A is an example of 13-element STZ that is prevalent in this 2D meshing. Region B is an exception that has 14 elements. Simple shear is applied when the sample is upon mechanical loading.
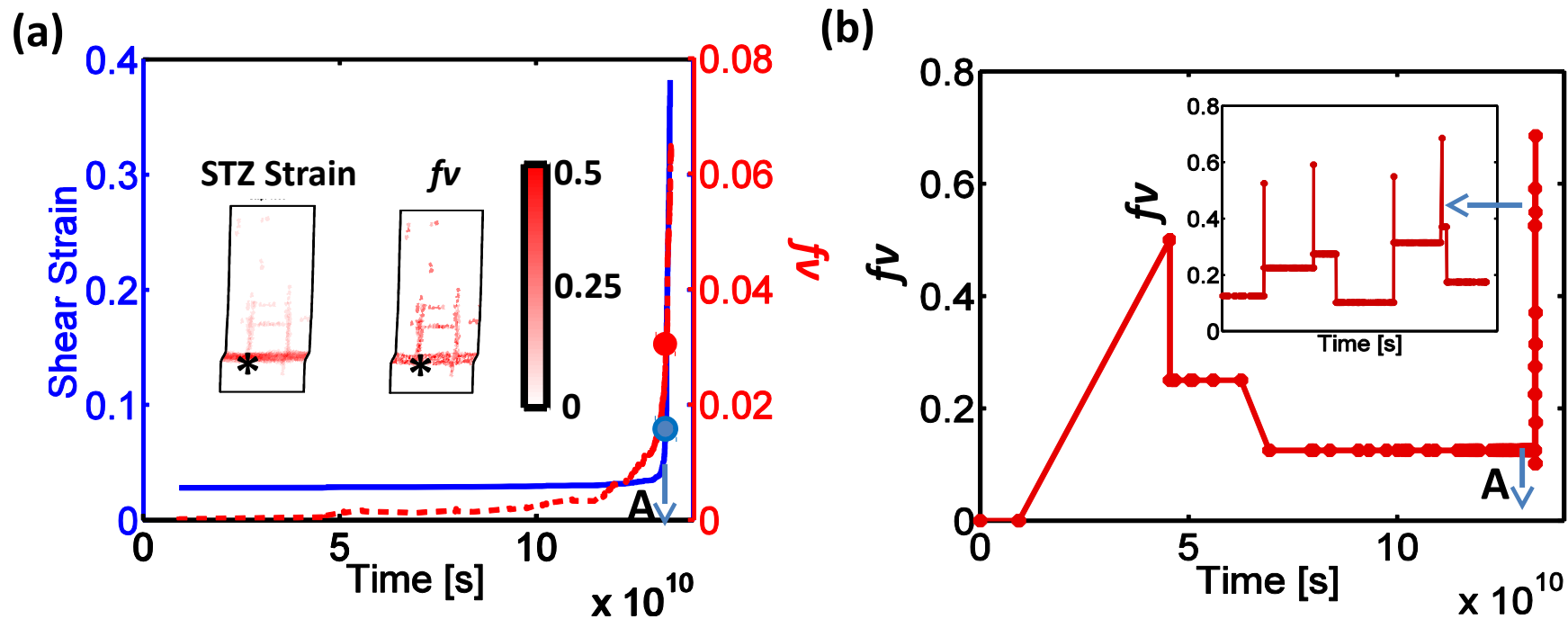
(a)

(b)

Fig. 2: (a) The macroscopic shear strain and excess free volume evolution with respect to time. The insets show the contour plot of the spatial distribution of plastic STZ strain and excess free volume at the time marked A. The position of the picked element is marked as a star in the contour plots. (b) The local excess free volume evolution of the selected element over a series of activation events (marked by the points). The inset is a magnified view at marker A. This test is conducted at constant shear = 1GPa and 300K upon a stress-free sample.

(a)

(b)
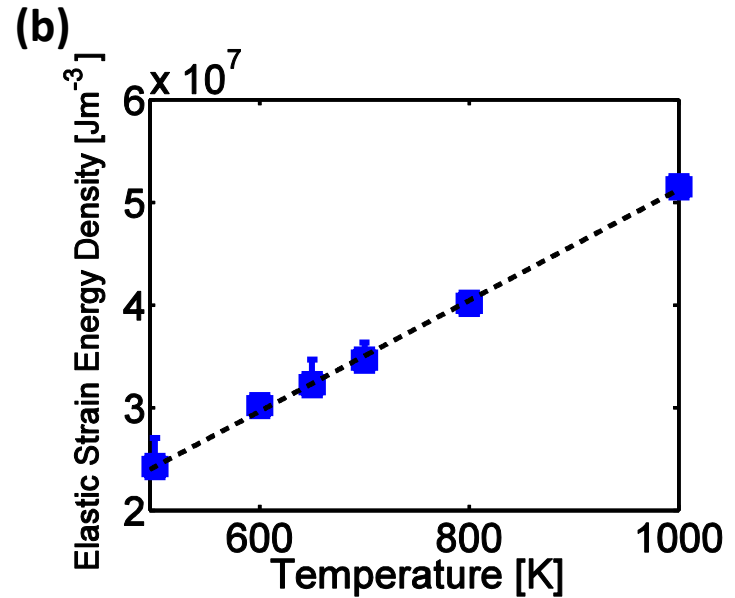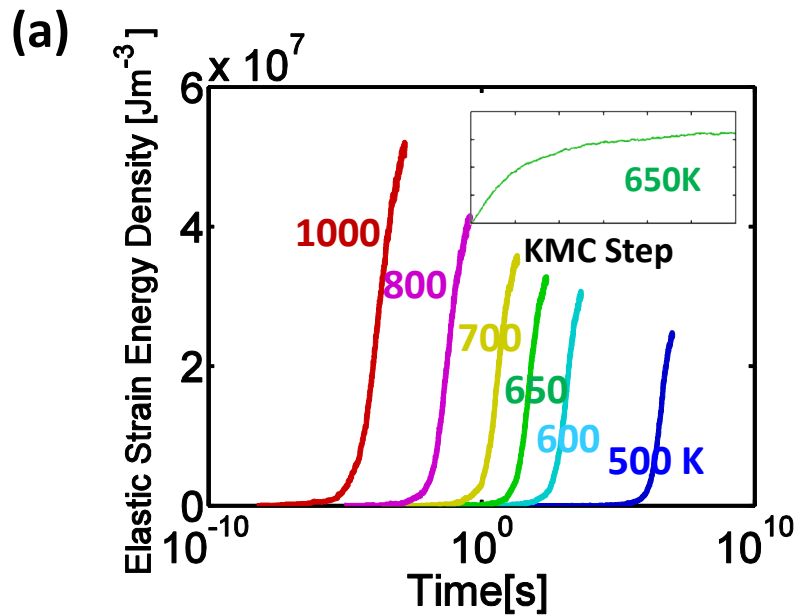
Fig. 3: (a) The elastic strain energy vs. time for annealing at various temperatures. Inset shows an example at 650K to confirm the convergence of this process to a steady state. (b) The elastic energy density at equilibrium state vs. temperature. A linear trend can be well established, which extends to 0 at 0K.
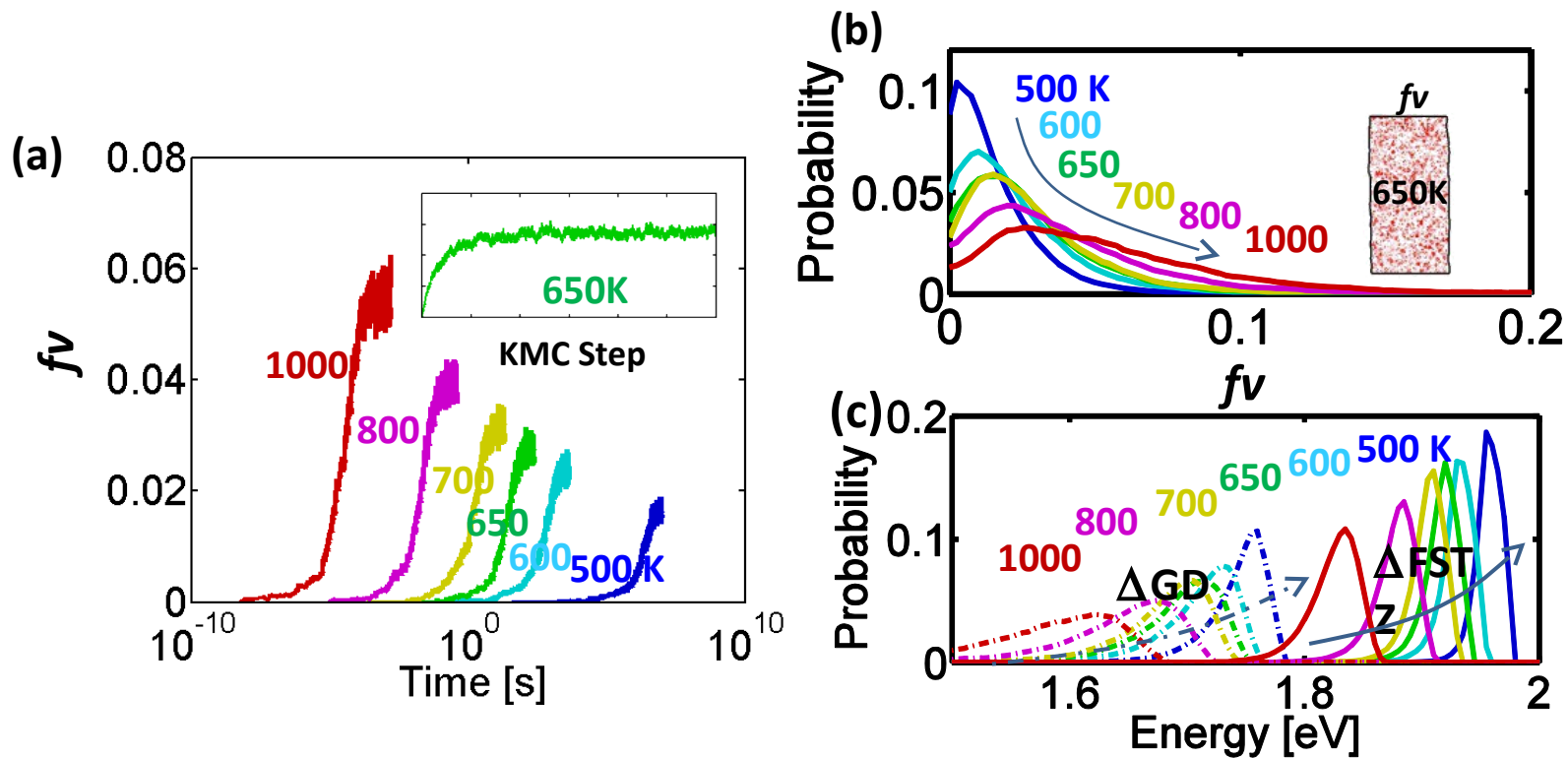
Fig. 4: (a)The evolution of excess volume average free volume fraction vs. time during simulated annealing at various temperatures. The inset shows an example at 650 K. (b) The distribution of excess free volume of each STZ when reaching steady state at various temperatures. Inset shows an example of the spatial distribution of fv at 650 K. (c) The activation energy distribution at steady state of various temperature for STZ activation, ΔFSTZ and diffusive arrangement ΔGD.
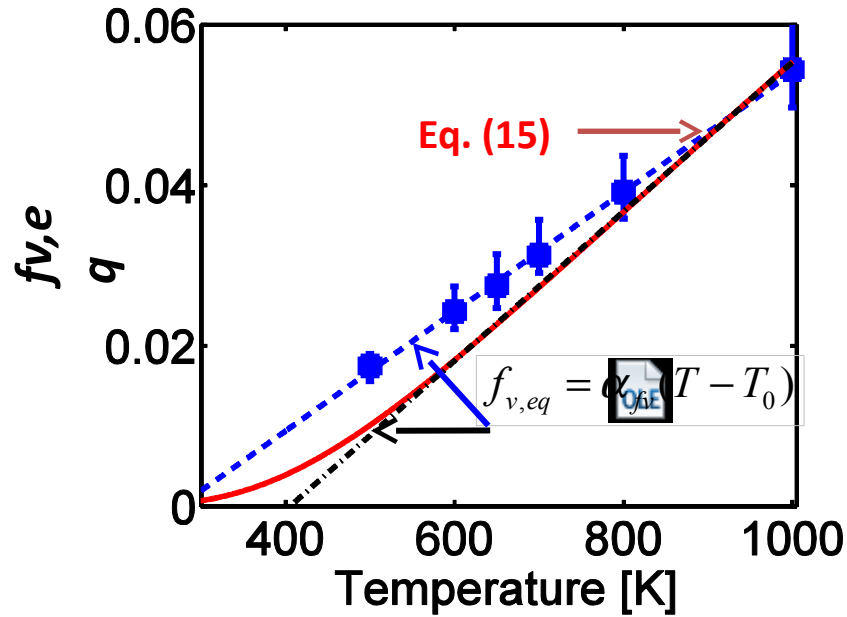
Fig. 5: The equilibrium free volume at various temperatures from annealing simulations, plotted along with a linear fitting fv = αfv(T-T0) , where αfv = 7.44 x 10-5 K-1 and T0 = 280 K. The numerical solution of Eq. (15) is shown in red; and its linearization is in black with αfv = 9.43 x 10-5 K-1 and T0 = 405 K calculated from Eq. (16) with f_{v0}=5%
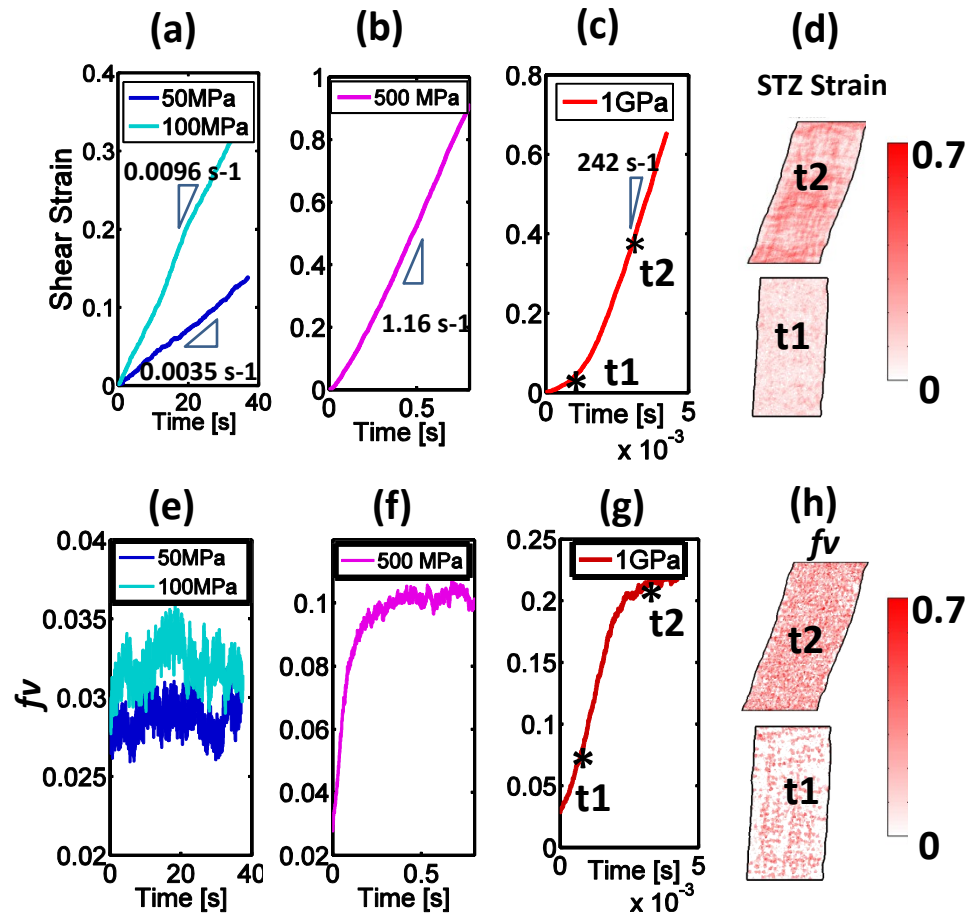
Fig. 6: (a)-(c) The strain vs. time data for the creep response of equilibrated structure upon various shear stresses at constant temperature 650K. (d) A snapshot is provided in (c) for the case of high shear stress = 1GPa at marked time, where the inset shows the physical deformation along with the magnitude of plastic STZ strains which are shaded. (e)-(g) The volume average excess free volume vs. time for the corresponding creep tests on the relaxed structure at 650K at various shear stresses. (h) Snapshots are provided at marked time in (g), where the inset shows the physical deformation along with the magnitude of excess free volume which are shaded.
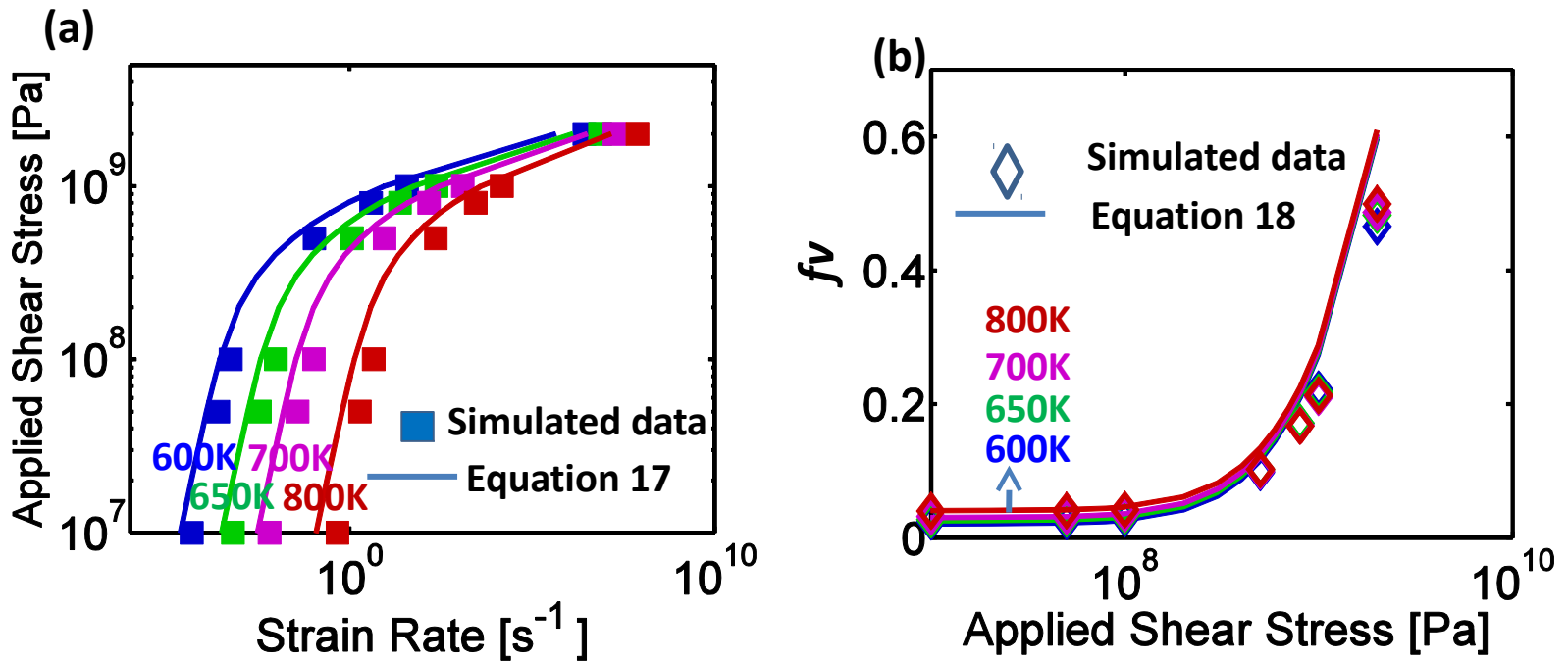
Fig. 7: (a) Steady-state homogenous flow data for several high temperature simulations, plotted along with the predicted strain rate of Eq.(17). (b) The equilibrium fv at steady-state as a function of applied load for several high temperature simulations, plotted along with the predicted values from Eq.(18).
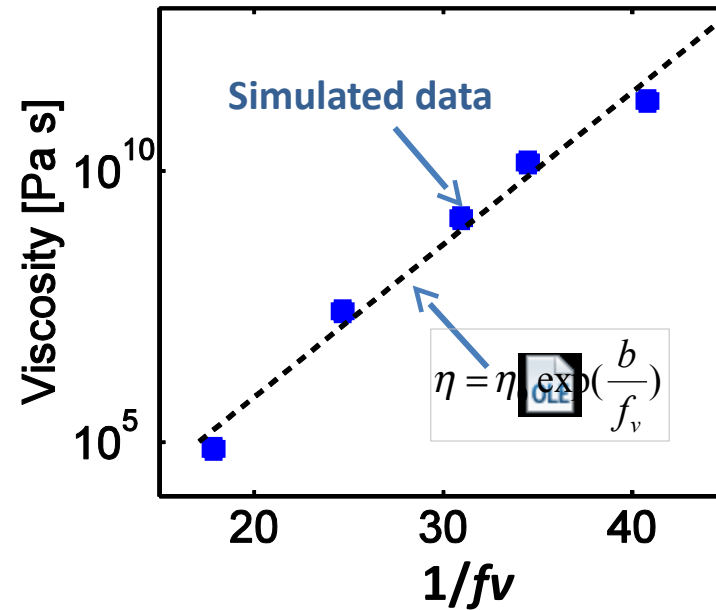
Fig. 8: The simulated viscosity in the Newtonian flow region at various temperatures vs. the corresponding excess equilibrium free volume fv , plotted along with the fitted Doolittle equation, $\eta = \eta_0 * \exp(b/fv)$, where $\eta_0 = 1.58$ and $b = 0.64$.
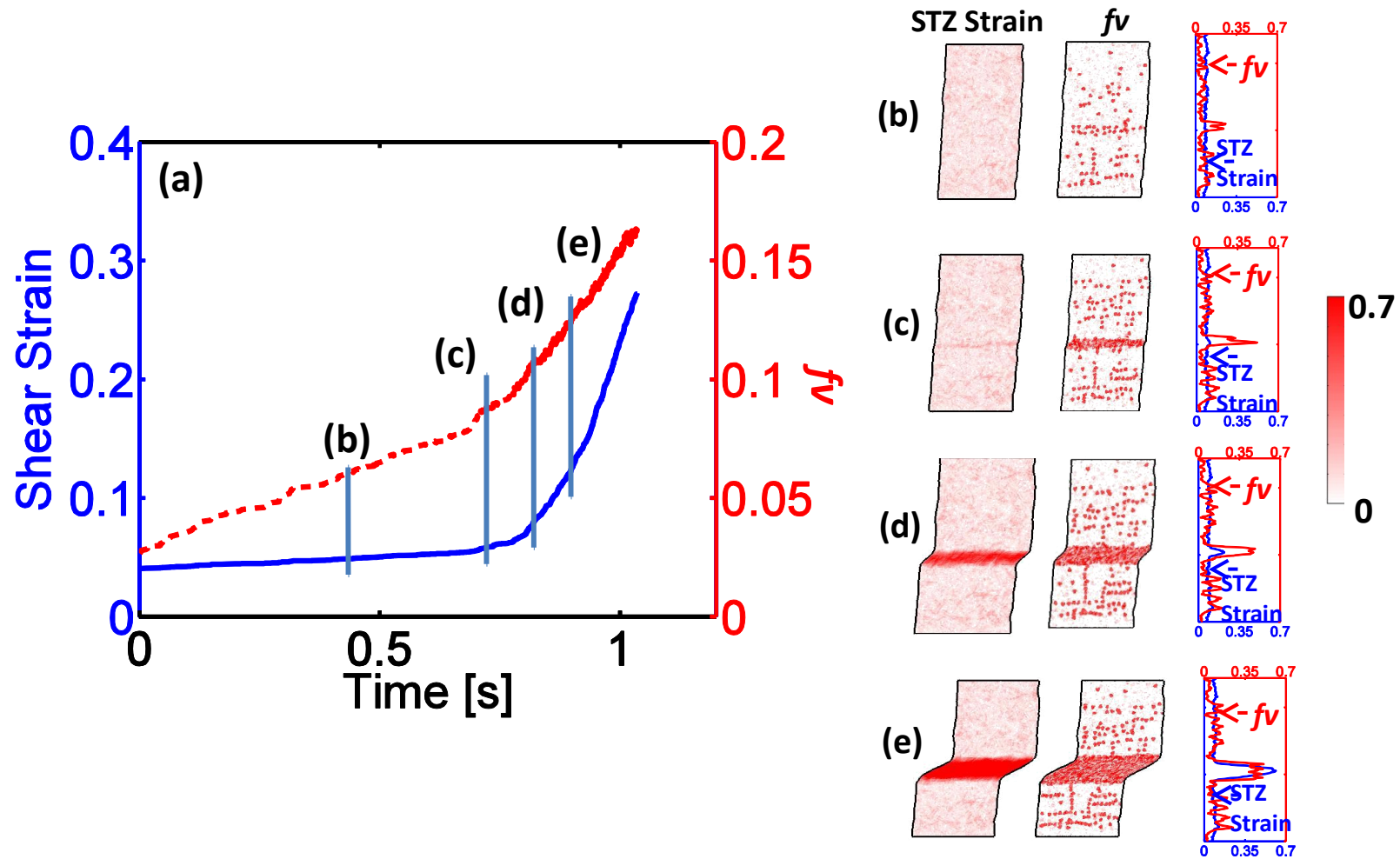
Fig. 9: (a) Volume average shear strain and excess free volume evolution vs. time of a cooled structure deformed at 300K and at 2GPa shear load. (b)- (e) correspond to the snapshots of the cooled structure at different time during the creep test. For each time, the physical deformation along with the magnitude of STZ strain or *fv* is plotted, and also 1D STZ and *fv* distributions along vertical direction are provided.
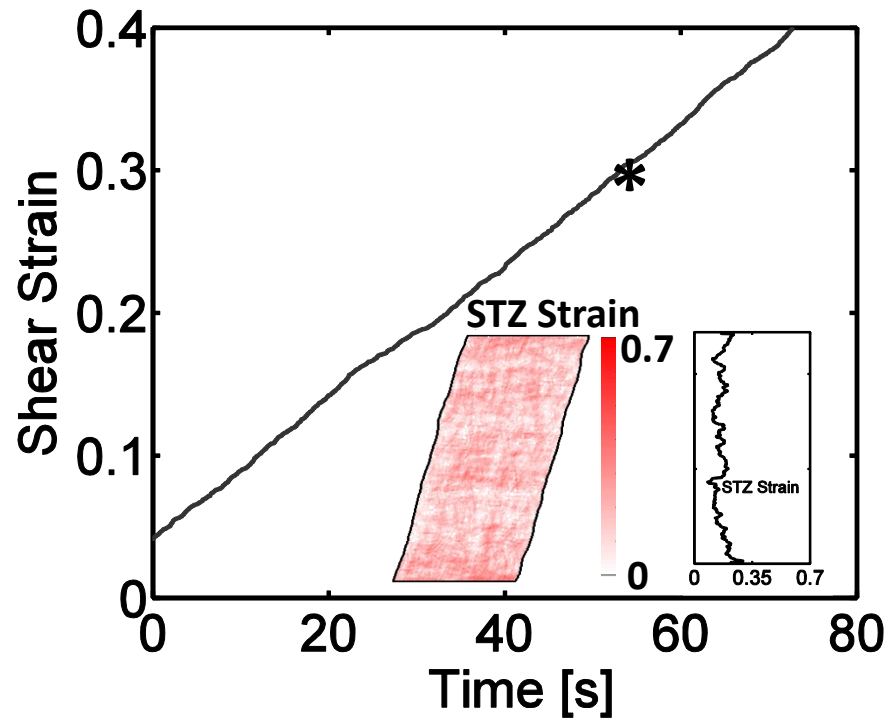
Fig. 10: Volume average shear strain vs. time of a cooled
structure deformed at 300K and at 2GPa shear load without
implementing free volume processes. Insets show the spatial
distribution of STZ strain and its corresponding 1D profile
along vertical direction at marked time, which illustrate the
homogenous nature of deformation.